ACS NANO

www.acsnano.org

ARTICLE

Co_3O_4 Nanosheets as Battery-Type Electrode for High-Energy Li-Ion Capacitors: A Sustained Li-Storage *via* Conversion Pathway

Palanichamy Sennu, Srinivasan Madhavi, Vanchiappan Aravindan,* and Yun-Sung Lee*

Cite This: *ACS Nano* 2020, 14, 10648−10654

Read Online

ACCESS | Metrics & More | Article Recommendations | Supporting Information

ABSTRACT: We report the excellent charge storage performance of high-energy Li-ion capacitors (LIC) fabricated from the mesoporous Co_3O_4 nanosheets as the conversion-type battery component and Jack fruit (*Artocarpus heterophyllus*) derived activated carbon as a supercapacitor electrode, especially at high temperatures (50 and 40 °C). Prior to the fabrication, the electrochemical prelithiation strategy was applied to Co_3O_4 to alleviate the irreversibility and enrich the Li-ions for electrochemical reactions ($Co^0 + Li_2O$). The LIC delivered a maximum energy density of ∼118 Wh kg^{-1} at a high temperature of 50 °C. The significant difference is observed at a high rate of 2.6 kW kg^{-1} at 50 °C with excellent cycle stability up to 3000 cycles, with a retention of ∼87% compared with the LIC cycled at room temperature (∼74%). The magnificent electrochemical performance clearly demonstrates that the mesoporous structure and residual carbon synergistically facilitated the Li^+/electron transport and hinder undesirable side reactions with electrolytes to realize high-energy density at high temperatures.

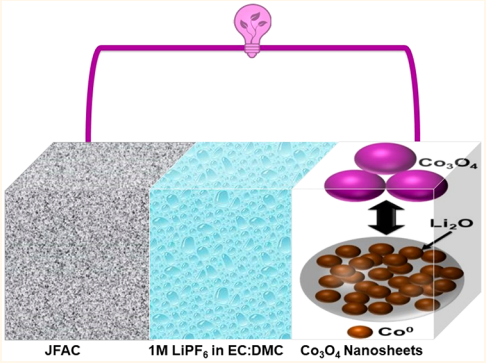

KEYWORDS: *Li-ion capacitor, high temperature, conversion reaction, stability, biomass*

The development of high-energy and high-power charge storage systems is desperately warranted to fulfill the demand to drive zero-emission transportations like electric vehicles (EV) and hybrid electric vehicles (HEV). The conventional rechargeable batteries, for example, Li-ion batteries (LIB) fail to translate the necessary power to the system due to the limited Li-ion diffusion kinetics. On the other hand, the supercapacitors (electric double-layer capacitors, EDLC) are unable to store the necessary energy owing to the non-Faradaic charge storage mechanism, though it offers the high-power capability (>10 kW kg^{-1}). This eventually leads to the exploration of different kinds of charge storage systems that can offer both high-energy and high-power capability. In this regard, Amatucci *et al.*[1] introduced the concept of integrating both high-energy LIB and high-power supercapacitors into the single system called Li-ion hybrid capacitor or Li-ion capacitor (LIC). Generally, in LIC assembly, the supercapacitor component is responsible for the power capability, whereas the battery-type electrode is accountable for boosting the energy density. In other words, the LIC involves the two different charge storage mechanisms, namely Faradaic and non-Faradaic processes. Theoretically, the LIC should exhibit higher energy and power capability than conventional LIB and EDLCs.[2,3] However, in practical systems, the LIC renders the necessary power but seriously suffers in the energy aspect. This is mainly due to the limited Li-ion kinetics associated with the insertion-type electrodes proposed and explored. Also, the higher Li-insertion potential into the battery-type component is worth mentioning.[4] On the other hand, high surface area activated carbon (AC) is the unanimous choice to be employed as an EDLC-type component.[5,6] Although, a few attempts like heteroatom doping, surface functionalization, graphene nanostructures, porous carbons, *etc.* have been carried out on the capacitor-type electrode to improve the performance.[6−8] However, aforementioned attempts yielded a marginal enhancement in the electrochemical activity in both the power and energy aspects. Further, the improvement in the energy is not at all sufficient for practical applications. Therefore, a highly efficient and high-performing battery-type electrode is necessary to

Received: June 14, 2020
Accepted: July 27, 2020
Published: July 27, 2020

https://dx.doi.org/10.1021/acsnano.0c04950
ACS Nano 2020, 14, 10648−10654

bring the commercial reality for LIC, especially looking for the better battery-type electrode beyond insertion mechanism.

Several transition-metal-based insertion-type materials like $Li_4Ti_5O_{12}$, $LiCrTiO_4$, V_2O_5, TiP_2O_7, $TiNb_2O_7$, TiO_2, $LiTi_2(PO_4)_3$, *etc.* are proposed to improve the energy density of the LIC which we described extensively in our review.[4] All of the insertion-type battery materials exhibited decent energy density (30 to 70 Wh kg^{-1}) and satisfactory electrochemical performance. However, the higher Li-insertion potential (>1.5 V vs Li) and limited reversible capacity (<200 mAh g^{-1}) hinder the potential use of the aforementioned materials. The well-known, state-of-the-art graphite can be employed as a potential battery-type electrode for the LIC configuration in the prelithiated (LiC_6) state.[9,10] However, the LIC is known for its high current operation, which eventually leads to the Li-platting and subsequent dendrite formation on the surface while employing graphitic anode. Hard carbon is considered as a tailor-made electrode for the LIC applications owing to the high rate capability and higher operating potential (>0.3 V *vs* Li) than graphite, which mostly escalates the Li-dendritic formation upon high current operation.[7,11] Although, the LIC prototypes available on the commercial market with prelithiated hard carbon anode and AC cathodes still suffer to achieve the high-energy density.[12,13] This is mainly because of the limited Li-ion kinetics with lower reversible capacity (<350 mAh g^{-1}). Similar to LIB, the concept of utilizing alloying and conversion material is proposed for the LIC perspective.[14,15] Among the alloy-type materials proposed, Si- and Sn-based derivatives are worth mentioning due to the higher reversible capacity (>600 mAh g^{-1}) and lower working potential (<0.3 V *vs* Li).[14−16] Unfortunately, the large volume variation (>200%), unstable solid-electrolyte interphase (SEI) formation, and poor cycling profile certainly prohibit the potential use. Also, there is a meagre possibility of Li-dendrite formation upon high-rate cycling owing to the lower working potential.[2] On the other hand, the higher operating potential (>0.5 V *vs* Li), high reversible capacity (>600 mAh g^{-1}), and less volume variation than alloy-type anodes make conversion-type electrodes potential candidates toward the fabrication of high-energy LIC.[17] In particular, Co_3O_4, which involves an eight electron reaction, yields the theoretical capacity of ∼890 mAh g^{-1}.[15,18−23] The redox potential of ∼1 V *vs* Li clearly falls within the safer thermodynamic stability window of the conventional carbonate-based electrolytes, and it is an added advantage compared to the alloy-type anodes. Further, it is well established that the nanostructured material is preferred for the case of conversion and alloy-type anodes, which involves complete participation of active material in the electrochemical reaction than bulk.[24,25] In this line, we made an attempt to explore the possibility of synthesizing the mesoporous two-dimensional Co_3O_4 nanosheet (NS) by a simple hydrothermal reaction. We anticipate that the presence of a porous structure and carbon layer could facilitate the high rate capability to the system, which obviously leads to realizing the LIC with high energy and power capability. Initially, we assessed the Li storage capability of Co_3O_4-NS in a half-cell assembly *vs* Li. The prelithiated form of Co_3O_4-NS was employed as a battery-type electrode with an AC counter electrode in LIC under the optimized mass loading conditions. The AC/prelithiated Co_3O_4-NS assembly displayed as the maximum energy density of ∼116.3 Wh kg^{-1} at room temperature (25 °C). Besides the ambient performance, an exceptional elevated temperature performance is noted and described in detail.

RESULTS/DISCUSSION

The X-ray diffraction (XRD) pattern of the synthesized Co_3O_4-NS and JFAC is shown in Figures 1a and S1a. Figure

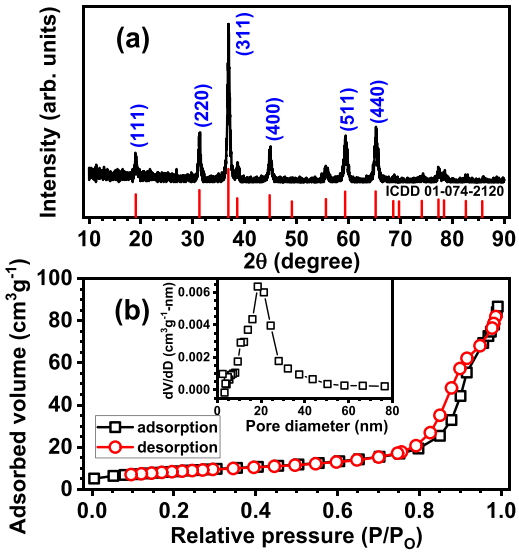

Figure 1. (a) XRD and (b) BET specific surface area of Co_3O_4 NSs (inset is pore size distribution).

1a, the sharp diffraction peaks positioned at $2\theta \approx 31.4$, 36.7, 44.7, 59.5, and 65.3° demonstrating the spinel phase of Co_3O_4 (ICSD 98-002-4210) with space group *Fd*3*m*. The high-intense reflections suggest the highly crystalline nature of the synthesized material phase. On the other hand, in Figure S1a, the two broad reflection peaks observed for JFAC from $2\theta \approx$ 14−30 and 38−48 corresponds to the characteristic (002) and (101) planes, and it corresponds to the amorphous in nature of the carbonaceous materials. The N_2 adsorption−desorption isotherms of Co_3O_4-NS and JFAC were investigated from the Brunauer−Emmett−Teller (BET) method, and the results are illustrated in Figures 1b and S1b. The specific surface area of Co_3O_4-NS was found to be 99.743 m^2 g^{-1}, and the isotherms belong to type-II isotherms with the H_3 hysteresis loop of IUPAC classification. This clearly confirms the presence of large mesopores with a Barret−Joyner−Halenda pore-size distribution of ∼20 nm (shown inset in Figure 1b). On the other hand, the shape of JFAC isotherms is completely different, which is mainly because of the chemical activation by using the KOH. Apparently, a significant uptake relatively at a low pressure of below P/P_o in the range of 0.05 belongs to the type-IV isotherm, which is associated with the mixed nature of meso- and microporosity. The BET specific surface area of the JFAC is calculated to be ∼2351 m^2 g^{-1}.

The morphological features of Co_3O_4-NS and JFAC were analyzed from FE-SEM and HR-TEM and are shown in Figures 2 and S2. The synthesized Co_3O_4 are nearly rectangle-shaped sheet-like structured dimensions of 3−7 μm, and the thicknesses are around 70−90 nm (Figured 2a,b and S2a,b). The widespread network morphology of Co_3O_4-NS is assembled from the numerous, randomly oriented nanoparticles in the size of 17−25 nm, coated and well connected by the polymer derived carbons (Figure 2c,d). Furthermore, we examined the microscopic structure of Co_3O_4-NS characterized by HR-TEM as shown in Figure 2e,f. The measured lattice spacings of 0.245 and 0.276 nm correspond to

https://dx.doi.org/10.1021/acsnano.0c04950
ACS Nano 2020, 14, 10648−10654

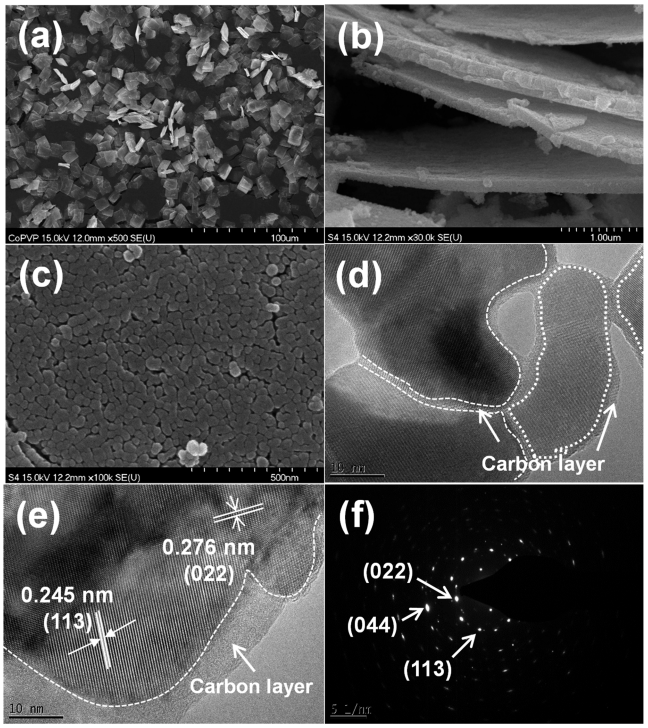

Figure 2. (a–c) FE-SEM and (d–f) HR-TEM images of the synthesized Co_3O_4 NSs.

the interlayer spacing of (113) and (022) crystal planes. The appearance of dot spots in the selected area electron diffraction (SAED) pattern of Co_3O_4-NS signifies the polycrystalline nature and can be parallel to the cubic spinel phase. Figure S3 shows the FE-SEM image of JFAC present in irregular granules format and leads to increases in the contact surface area, which facilitates the fast charge transfer and high capacity. Obviously, the morphology of the JFAC is consistent with the surface features of the biomass-derived ACs.[6] Upon the calcination of Co_3O_4-NS, the decomposition of the PVP leads to the formation of the carbonaceous layer. The temperature 400 °C is not sufficient to completely remove the trace amount of carbonaceous content. Nevertheless, the presence of such a trace amount of leftover carbon is certainly beneficial to the electrochemical activity of Co_3O_4-NS in terms of better particle connectivity and facile electron transport. Also, the amorphous carbon is known to sustain the volume variation observed during the conversion reaction. Thermogravimetric analysis was performed to estimate the amount of carbon present in the Co_3O_4 and was estimated to be 0.46 wt % (Figure S4).

Figure 3 represents the Li-storage properties of the Co_3O_4-NS in half-cell assembly (*vs* Li) at the current density of the 100 mA g^{-1}. Prior to the fabrication of the LIC, the assessment of Li-storage properties of the battery-type materials is essential to ensure the reversibility and mass balance. As mentioned earlier, the Co_3O_4 is a perfect example of the conversion-type material category, which undergoes an eight electron reaction. Accordingly, the Li/Co_3O_4-NS half-cell delivered a capacity of ~2270 and ~1242 mAh g^{-1} for first discharge and charge, respectively. This corresponds to a coloumbic efficiency of ~55%, which is expected for the case of conversion-type negative electrodes. The half-cell displayed multiple short plateaus, and these regions correspond to the various electrochemical reactions upon the first deep discharge. The

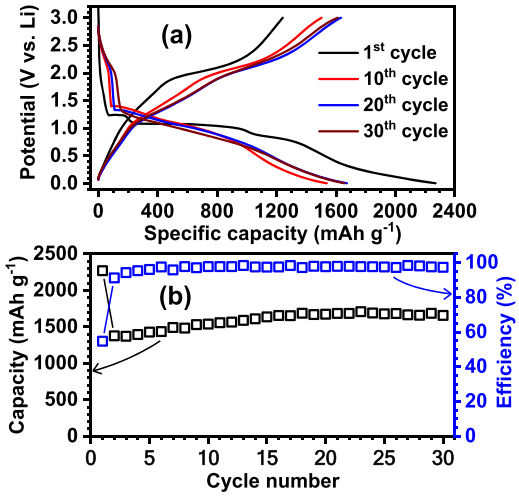

Figure 3. (a) Galvanostatic charge–discharge and (b) cycling profile (discharge capacity) of Co_3O_4-NS in a single-electrode (half-cell) configuration between 0.05 and 3 V *vs* Li at a current rate of 0.1 A g^{-1}.

cell potential of ~1.24 V *vs* Li is associated with the irreversible Li-insertion into the Co_3O_4 ($Li_{1.86}Co_3O_4$). Further, the long distinct plateau observed at ~1.08 V *vs* Li corresponds to the structural destruction of the above said lithiated phase ($Li_{1.86}Co_3O_4$), in other words, the formation of electrochemically generated metallic nanoparticle (Co^0) in the amorphous Li_2O phase or conversion of metal oxide into the metallic phase ($Li_{1.86}Co_3O_4 + 6.14Li^+ + 6.14e^- \rightarrow Co^0 + 4Li_2O$). Also, a small distinct plateau is also evident at ~0.84 V *vs* Li due to the decomposition of the conventional carbonate-based electrolyte solution and subsequent formation of the SEI layer. This SEI layer is composed of inorganic byproducts like LiF, Li_2CO_3, *etc.*, along with the polymeric moieties as well.[26,27] The formation of stable SEI is one of the important criteria to establish a high-performance anode, which often consumes the Li-ions in an irreversible manner. This irreversible consumption results in the inferior coloumbic efficiency in the first cycle. On the other hand, a broad peak located at ~2.02 V *vs* Li is evident upon the charging process, which corresponds to the oxidation of the metal to metal oxides ($Co^0 \rightarrow Co_3O_4$).[28,29] The intercalation, conversion, and oxidation potentials during the electrochemical charge–discharge process are clearly seen from the differential capacity profile (Figure S5). The half-cell delivered the capacity of ~1376 and ~1255 mAh g^{-1} for second discharge and charge, respectively, with a coloumbic efficiency of ~91.2%. Compared to the first cycle, a dramatic improvement in the reversibility is noted for the second cycle. A highly stable cycling profile is observed for Co_3O_4-NS in the half-cell assembly; for example, the cell delivered a discharge capacity of ~1657 mAh g^{-1} after 30 cycles. The observed capacity is higher than the theoretical limitations of the eight electron reaction in which the contribution of the capacity from the interfacial or SEI layer is worth mentioning. The marginal increase in the capacity, compared to the second cycle, is due to the complete participation of the active material in the electrochemical reaction. This complete participation could be enabled because of the porous morphology of the Co_3O_4-NS, which facilitates the electrolyte flow. As a result, active material will be exposed more toward the electrolyte solution and formation of the stable SEI layer. It is worth mentioning that the presence of a

https://dx.doi.org/10.1021/acsnano.0c04950
ACS Nano 2020, 14, 10648–10654

trace amount of carbon is one of the beneficial factors to form the stable SEI layer and also sustain the volume variation observed upon the charge−discharge processes. This stable SEI layer not only translates a better electrochemical activity but also tends to contribute the capacity through the interfacial layer.[30] Overall, the battery-type Co_3O_4-NS rendered satisfactory Li-storage properties in terms of high capacity and stability and ensured the suitability to be employed toward the fabrication of LIC.

Similar to Li-storage capability assessment of the battery-type Co_3O_4-NS, the supercapacitor component, JFAC, was also subjected to study this environment to foresee the feasibility to pair. The JFAC was prepared from the *Artocarpus heterophyllus* biomass, and the procedure is described in detail in our previous work.[31] Accordingly, the half-cell was fabricated and studied at a current density of 100 mA g^{-1}, as shown in Figure S6. The existence of a linear charge−discharge curve clearly confirms the reversible formation of a double layer across the electrode−electrolyte interface. The half-cell delivered the capacity of ∼140 mAh g^{-1} with a coloumbic efficiency of >99%. Apparently, the JFAC is an excellent EDLC component to couple with Co_3O_4-NS in LIC assembly. Another important point to mention here is that the Co_3O_4-NS exhibits a large irreversibility in the first cycle and also requires a prelithiation to provide necessary Li-ions for the electrochemical reaction in a wider operating potential.[14] In the LIC assembly, the source of Li-ion is highly limited, whereas in a half-cell, metallic Li serves as a reservoir for Li-ions. Hence, the Co_3O_4-NS is prelithiated by conducting the three complete charge−discharge cycles and dismantled in the discharged state (Co^0 + Li_2O).[32] Based on the electrochemical performance of both Co_3O_4-NS and JFAC in half-cell assembly with Li, the mass loading between the anode to cathode is fixed at the ratio of 1:10.

The LIC is fabricated with prelithiated Co_3O_4-NS as a battery-type component and JFAC as EDLC-type electrode under the balanced mass loading conditions (15 mg). Here, the applied current rate, energy, and power density are calculated based on the total mass loading of the active materials, that is, Co_3O_4-NS and JFAC. The LIC was tested between 1 and 3.5 V at various scan rates and current densities and is shown in Figure 4. From the cyclic voltammetry (CV) traces, the sudden increase in the current at a higher potential is due to the redox reaction of the battery-type component involved in the electrochemical reaction. This clearly confirms that LIC undergoes both a Faradaic and non-Faradaic process. More clearly, upon the charge−discharge process, the anions present in the electrolyte solution (PF_6^-) adsorbed/desorbed on the JFAC surface and eventually formed the double layer across the interface. The battery-type component was used in the discharged state (Co^0 and Li_2O); the formation of Co_3O_4 is observed during the charging process, whereas the reconversion into a metallic state happens at the discharge process. The same behavior is observed for all the three cells measured at different temperature conditions (Figures S7 and S8). To further understand, the galvanostatic charge−discharge studies were conducted, and profiles are given in Figure 4. The distortion in the linear charge−discharge curve corresponds to the LIC involved in two different charge storage mechanisms, and the same trend is noted for the other two temperature conditions (25 and 40 °C) as well. In all cases, an increase in the current applied rate tends to decrease the discharge time, which is generally expected. At higher

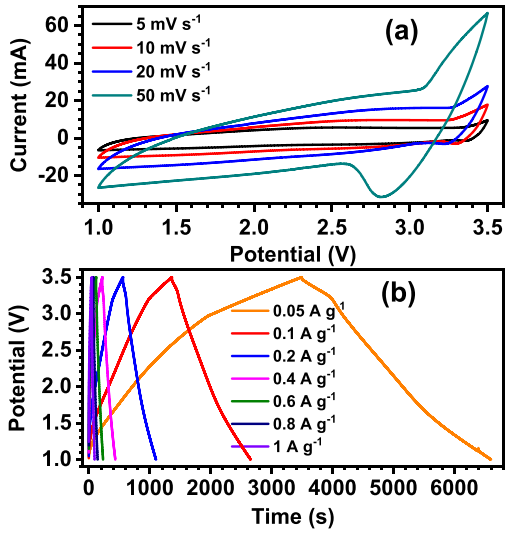

Figure 4. (a) CV traces at various scan rates and (b) galvanostatic charge/discharge profile of Co_3O_4-NS/JFAC-based LIC at various current densities recorded between 1 and 3.5 V at 50 °C.

current rates, the complete participation of active materials is limited for the Faradaic reaction.[33] Hence, the decrease in the discharge time is registered, and it is quite normal for any charge storage system.

Electrochemical impedance spectroscopy (EIS) study is one of the versatile techniques to understand the nature of the interfacial behavior across the electrode and electrolyte interphase and illustrated as a Nyquist plot in Figure 5. In

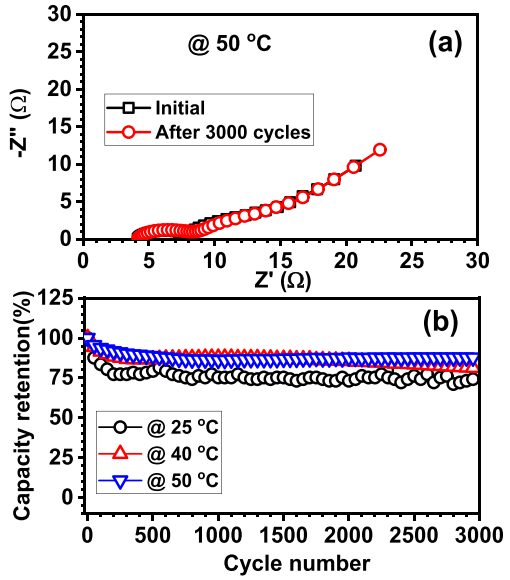

Figure 5. (a) Comparison Nyquist plots of Co_3O_4-NS/JFAC-based LIC cycled at 50 °C before and after 3000 cycles. (b) The cycling profile of LIC at different temperatures recorded at a current density of 0.2 A g^{-1} between 1 and 3.5 V.

the Nyquist plot composed of three main regions, in which the high-frequency region corresponds to the solution resistance, the medium frequency range is associated with the charge-transfer resistance (R_{CT}), and the low-frequency domain with the inclined at 45° vertical tail is referred as a Warburg impedance. This Warburg tail is always used to understand the

https://dx.doi.org/10.1021/acsnano.0c04950
ACS Nano 2020, 14, 10648−10654

diffusion-controlled process or kinetically controlled storage process. The EIS traces were recorded before and after 3000 cycles for all the three temperature conditions. Obviously, there is not much deviation observed for the LIC's tested at 40 and 50 °C, whereas a drastic reduction in the R_{CT} is observed for 25 °C. However, prior to the EIS measurement, the cells were aged for 1 h to ensure stabilization. After 3000 cycles, the SEI layer becomes conductive at 25 °C, which is evident from the EIS traces. Cycling stability is one of the prime aspects of each and every charge-storage system. In this line, the cycling stability of the prelithiated Co_3O_4-NS and JFAC-based LIC were tested at a current density of 200 mA g^{-1} and is shown in Figure 5b. The obtained capacity of all the three temperature conditions was normalized and compared. After 3000 cycles, the LIC rendered ~87, ~81, and ~74% of retention at 50, 40, and 25 °C, respectively. Notably, ~7% higher retention is noted for the case of conversion-type Co_3O_4-NS-based assembly. Also, most of the active material failed to translate the room-temperature electrochemical activity at high temperature, but in this case, we observed a much better performance at high-temperature conditions. This is quite interesting, and we strongly believe that the highly porous structure, 2D morphology, and appropriate mass balance between the supercapacitor and battery-type electrode are responsible for this superior performance. Further, studies are in progress to understand the exceptional performance of this fascinating system, particularly at elevated temperature conditions.

A Ragone plot is another important way to measure the power capability of the system with respect to energy density, as shown in Figure 6. Specific energy (E) and power densities (P) were calculated using the following relations: $P = (\Delta E \cdot i/m)$ and $E = (P \cdot t)$. As mentioned above, the total mass (m = 15 mg) of the active material has been considered for the calculation of energy and power densities. The average working potential (ΔE) is taken for the calculation, rather than the upper cutoff potential; a representative calculation of average working potential is given in Figure S9, in which the intersection of the charge−discharge curves is considered as the average working potential. I is applied current (A), and t represents discharge time (s) during the galvanostatic measurement. The LIC delivered more or less the same energy density at lower current rates, for example, ~118, ~122, and ~116 Wh kg^{-1} for 50, 40, and 25 °C, respectively. The obvious difference is noted at the higher rates, in which, as expected, at 50 °C, the LIC displayed an energy density of ~33 Wh kg^{-1}, whereas ~28 and ~18 Wh kg^{-1} are accounted for the cases of 40 and 25 °C, respectively. The observed performance at 50 °C is not only superior to those tested at various environments but also outperformed other configurations compared in the Ragone plot. High-temperature performance is one of the prerequisites to employ any charge storage system, and not only for this hybrid configuration toward EV and HEV applications.[34−37] Although the Co_3O_4-NS based LIC is completely fascinating, further studies like the influence, dimensionality, composite formulation, and subzero temperature performance are essential prior to commercialization.

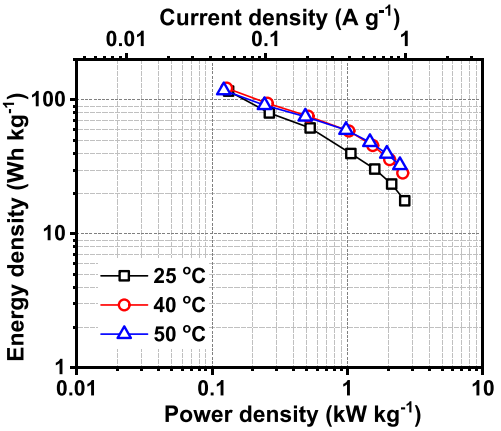

Figure 6. Ragone plot of Co_3O_4-NS/JFAC-based LIC at various temperature conditions.

CONCLUSIONS

We successfully demonstrated the fabrication of high-energy LIC with exceptional electrochemical performance using the conversion-type battery electrode, especially at elevated temperatures. The presence of mesoporosity and a trace amount of carbon leftover during the synthesis was certainly beneficial to realize the better performance. Further, the synergistic support from the supercapacitor-type electrode, JFAC, and an appropriate mass loading between the electrodes was very crucial to achieve such high-energy density and stability. The prelithiated Co_3O_4/JFAC-based LIC delivered the maximum energy density of 118 Wh kg^{-1} with an excellent capacity retention of ~87% after 3000 cycles at 50 °C. Overall, this study provides an opportunity for the exploration of a conversion-type negative electrode in hybrid configuration toward commercial reality.

METHODS

Synthesis of Co_3O_4 Nanosheets and Jack Fruit Activated Carbon. The mesoporous Co_3O_4 NSs were synthesized by using a simple hydrothermal method described elsewhere.[38] In this procedure, 1 g of the hydrated form of cobalt chloride (Wako, Japan) and 4 g of urea (Junsei, Japan) were dissolved in distilled water. Further, 4 g of polyvinylpyrrolidone (MW = 40,000, Sigma-Aldrich, USA) powder was added into the above pink colored solution under constant stirring, and the solution pH became around 4. Then, the clear solution was transferred into a Teflon-lined stainless steel autoclave and heated at 120 °C for 4 h in a hot air oven. After the completion of the reaction, the final product washed several times with water/ethanol and then calcined at 400 °C for 3 h in the air atmosphere.

The dried pieces of jack fruit (JF) peels were charred at 200 °C for 4 h under the air atmosphere and then ground into a fine powder, as described in our previous work.[31] The black color JF powder was mixed with KOH (1:2 ratio), and after drying in a hot air oven, the mixture was activated at 900 °C for 3 h under N_2 atmosphere. The resultant product (pH: ~13) was washed several times with water and ethanol until the pH of the solution became neutral. The obtained powder was dried in the conventional oven at 80 °C overnight and designated as JFAC and subsequently used for further characterization.

Material Characterization and Electrode Preparation. The Rint 1000 X-ray diffractometer (Rigaku, Japan) with Cu Kα radiation was used to record the diffraction patterns of the synthesized Co_3O_4 and JFAC phases. The BET specific surface area measurements were performed with a ASAP 2010 surface analyzer (Micromeritics, USA). The morphological features of samples were examined with field-emission scanning electron microscopy (S-4700 microscope, Hitachi, Japan) and high-resolution transmission electron microscopy (TecnaiF20, Philips, Holland).

All the electrochemical performances of synthesized samples were studied in the CR2032 coin cells. The mixed slurry [72% active materials, 14% Ketjen black, and 14% Teflonized acetylene black] was

https://dx.doi.org/10.1021/acsnano.0c04950
ACS Nano 2020, 14, 10648−10654

pressed on to the 200 mm^2 stainless steel current collector and then dried at 160 °C for 4 h under vacuum conditions. The test cells were fabricated in an Ar-filled glovebox, and the lithium metal was used as the reference and counter electrode in a half-cell assembly. The Celgard 3401 polymer was used as the separator and 1 M $LiPF_6$ (1:1 v/v ethylene carbonate (EC): dimethyl carbonate (DMC), Soulbrain Co., Ltd., Korea) as the electrolyte solution. Electrochemical studies like CV, and ac impedance was carried out using an SP-150 electrochemical analyzer (Bio-Logic, France). The charge−discharge characteristics of the cells were evaluated at different temperatures of 25, 40, and 50 °C.

ASSOCIATED CONTENT

Supporting Information

The Supporting Information is available free of charge at https://pubs.acs.org/doi/10.1021/acsnano.0c04950.

The synthesized JFAC XRD and BET surface area, the SEM images of Co_3O_4 NSs, and JFAC. The CV, Nyquist plots, and the charge−discharge curves of LIC at 25 and 40 °C (PDF)

AUTHOR INFORMATION

Corresponding Authors

Yun-Sung Lee − *Faculty of Applied Chemical Engineering, Chonnam National University, Gwang-ju 500-757, Republic of Korea;* orcid.org/0000-0002-6676-2871; Email: leeys@chonnam.ac.kr

Vanchiappan Aravindan − *Department of Chemistry, Indian Institute of Science Education and Research (IISER), Tirupati 517507, India;* orcid.org/0000-0003-1357-7717; Email: aravind_van@yahoo.com

Authors

Palanichamy Sennu − *Faculty of Applied Chemical Engineering, Chonnam National University, Gwang-ju 500-757, Republic of Korea; School of Materials Science and Engineering, Nanyang Technological University, Singapore 639798; Singapore-HUJ Alliance for Research and Enterprise (SHARE), Nanomaterials for Energy and Energy-Water Nexus (NEW), Campus for Research Excellence and Technological Enterprise (CREATE), Singapore 138602*

Srinivasan Madhavi − *School of Materials Science and Engineering, Nanyang Technological University, Singapore 639798; Singapore-HUJ Alliance for Research and Enterprise (SHARE), Nanomaterials for Energy and Energy-Water Nexus (NEW), Campus for Research Excellence and Technological Enterprise (CREATE), Singapore 138602*

Complete contact information is available at: https://pubs.acs.org/10.1021/acsnano.0c04950

Notes

The authors declare no competing financial interest.

ACKNOWLEDGMENTS

Y.S.L. thanks the the National Research Foundation of Korea (NRF) for financial support through a grant funded by the Korea government (Ministry of Science, ICT & Future Planning) (no. 2019R1A4A2001527). V.A. acknowledges financial support from the Science & Engineering Research Board (SERB), a statutory body of the Department of Science & Technology (DST), Government of India, through the Ramanujan Fellowship (SB/S2/RJN-088/2016). S.M. thanks the financial support from the National Research Foundation, Prime Minister's Office, Singapore under its Campus of Research Excellence and Technological Enterprise (CREATE) program under the Singapore-HUJ Alliance for Research and Enterprise Ltd (SHARE), and NEW-CREATE which is joint research program between the Hebrew University of Jerusalem (HUJ, Israel) and Nanyang Technological University (NTU, Singapore).

REFERENCES

(1) Amatucci, G. G.; Badway, F.; Du Pasquier, A.; Zheng, T. An Asymmetric Hybrid Nonaqueous Energy Storage Cell. *J. Electrochem. Soc.* **2001**, *148*, A930.

(2) Plitz, I.; DuPasquier, A.; Badway, F.; Gural, J.; Pereira, N.; Gmitter, A.; Amatucci, G. G. The Design of Alternative Nonaqueous High Power Chemistries. *Appl. Phys. A: Mater. Sci. Process.* **2006**, *82*, 615−626.

(3) Pasquier, A. D.; Plitz, I.; Gural, J.; Badway, F.; Amatucci, G. G. Power-Ion Battery: Bridging the Gap between Li-Ion and Supercapacitor Chemistries. *J. Power Sources* **2004**, *136*, 160−170.

(4) Aravindan, V.; Gnanaraj, J.; Lee, Y.-S.; Madhavi, S. Insertion-Type Electrodes for Nonaqueous Li-Ion Capacitors. *Chem. Rev.* **2014**, *114*, 11619−11635.

(5) Bianco, A.; Chen, Y.; Frackowiak, E.; Holzinger, M.; Koratkar, N.; Meunier, V.; Mikhailovsky, S.; Strano, M.; Tascon, J. M. D.; Terrones, M. Carbon Science Perspective in 2020: Current Research and Future Challenges. *Carbon* **2020**, *161*, 373−391.

(6) Divya, M. L.; Natarajan, S.; Lee, Y.-S.; Aravindan, V. Biomass-Derived Carbon: A Value-Added Journey towards Constructing High-Energy Supercapacitors in an Asymmetric Fashion. *ChemSusChem* **2019**, *12*, 4353−4382.

(7) Natarajan, S.; Lee, Y. S.; Aravindan, V. Biomass-Derived Carbon Materials as Prospective Electrodes for High-Energy Lithium-and Sodium-Ion Capacitors. *Chem. - Asian J.* **2019**, *14*, 936−951.

(8) Gogotsi, Y. Not Just Graphene: The Wonderful World of Carbon and Related Nanomaterials. *MRS Bull.* **2015**, *40*, 1110−1121.

(9) Sennu, P.; Aravindan, V.; Ganesan, M.; Lee, Y. G.; Lee, Y. S. Biomass-Derived Electrode for Next Generation Lithium-Ion Capacitors. *ChemSusChem* **2016**, *9*, 849−854.

(10) Divya, M. L.; Natarajan, S.; Lee, Y.-S.; Aravindan, V. Achieving High-Energy Dual Carbon Li-Ion Capacitors with Unique Low- and High-Temperature Performance from Spent Li-Ion Batteries. *J. Mater. Chem. A* **2020**, *8*, 4950−4959.

(11) Jayaraman, S.; Jain, A.; Ulaganathan, M.; Edison, E.; Srinivasan, M.; Balasubramanian, R.; Aravindan, V.; Madhavi, S. Li-Ion *vs.* Na-Ion Capacitors: A Performance Evaluation with Coconut Shell Derived Mesoporous Carbon and Natural Plant Based Hard Carbon. *Chem. Eng. J.* **2017**, *316*, 506−513.

(12) Naoi, K.; Naoi, W.; Aoyagi, S.; Miyamoto, J.-i.; Kamino, T. New Generation "Nanohybrid Supercapacitor. *Acc. Chem. Res.* **2013**, *46*, 1075−1083.

(13) Naoi, K.; Ishimoto, S.; Miyamoto, J.-i.; Naoi, W. Second Generation 'Nanohybrid Supercapacitor': Evolution of Capacitive Energy Storage Devices. *Energy Environ. Sci.* **2012**, *5*, 9363−9373.

(14) Aravindan, V.; Lee, Y.-S. Building Next-Generation Li-Ion Capacitors with High Energy: An Approach beyond Intercalation. *J. Phys. Chem. Lett.* **2018**, *9*, 3946−3958.

(15) Aravindan, V.; Lee, Y.-S.; Madhavi, S. Research Progress on Negative Electrodes for Practical Li-Ion Batteries: Beyond Carbonaceous Anodes. *Adv. Energy Mater.* **2015**, *5*, 1402225.

(16) Beattie, S. D.; Larcher, D.; Morcrette, M.; Simon, B.; Tarascon, J. M. Si Electrodes for Li-Ion Batteries—A New Way to Look at an Old Problem. *J. Electrochem. Soc.* **2008**, *155*, A158.

(17) Aravindan, V.; Lee, Y.-S. Electrochemical Activity of Hematite Phase in Full-Cell Li-Ion Assemblies. *Adv. Energy Mater.* **2018**, *8*, 1702841.

(18) Badway, F.; Plitz, I.; Grugeon, S.; Laruelle, S.; Dollé, M.; Gozdz, A. S.; Tarascon, J. M. Metal Oxides as Negative Electrode Materials in Li-Ion Cells. *Electrochem. Solid-State Lett.* **2002**, *5*, A115.

(19) Wu, Z.-S.; Ren, W.; Wen, L.; Gao, L.; Zhao, J.; Chen, Z.; Zhou, G.; Li, F.; Cheng, H.-M. Graphene Anchored with Co_3O_4 Nanoparticles as Anode of Lithium Ion Batteries with Enhanced Reversible Capacity and Cyclic Performance. *ACS Nano* **2010**, *4*, 3187−3194.
(20) Wang, D.; Yu, Y.; He, H.; Wang, J.; Zhou, W.; Abruña, H. D. Template-Free Synthesis of Hollow-Structured Co_3O_4 Nanoparticles as High-Performance Anodes for Lithium-Ion Batteries. *ACS Nano* **2015**, *9*, 1775−1781.
(21) Wang, Y.; Xia, H.; Lu, L.; Lin, J. Excellent Performance in Lithium-Ion Battery Anodes: Rational Synthesis of $Co(CO_3)_{0.5}(OH)$-$0.11H_2O$ Nanobelt Array and Its Conversion into Mesoporous and Single-Crystal Co_3O_4. *ACS Nano* **2010**, *4*, 1425−1432.
(22) Huang, G.; Zhang, F.; Du, X.; Qin, Y.; Yin, D.; Wang, L. Metal Organic Frameworks Route to *In Situ* Insertion of Multiwalled Carbon Nanotubes in Co_3O_4 Polyhedra as Anode Materials for Lithium-Ion Batteries. *ACS Nano* **2015**, *9*, 1592−1599.
(23) Adekoya, D.; Chen, H.; Hoh, H. Y.; Gould, T.; Balogun, M. S. J. T.; Lai, C.; Zhao, H.; Zhang, S. Hierarchical Co_3O_4@N-Doped Carbon Composite as an Advanced Anode Material for Ultrastable Potassium Storage. *ACS Nano* **2020**, *14*, 5027−5035.
(24) Aricò, A. S.; Bruce, P.; Scrosati, B.; Tarascon, J.-M.; van Schalkwijk, W. Nanostructured Materials for Advanced Energy Conversion and Storage Devices. *Nat. Mater.* **2005**, *4*, 366−377.
(25) Poizot, P.; Laruelle, S.; Grugeon, S.; Dupont, L.; Tarascon, J. M. Nano-Sized Transition-Metal Oxides as Negative-Electrode Materials for Lithium-Ion Batteries. *Nature* **2000**, *407*, 496−499.
(26) Xu, K. Electrolytes and Interphases in Li-Ion Batteries and Beyond. *Chem. Rev.* **2014**, *114*, 11503−11618.
(27) Kim, Y.; Lee, J.-H.; Cho, S.; Kwon, Y.; In, I.; Lee, J.; You, N.-H.; Reichmanis, E.; Ko, H.; Lee, K.-T.; Kwon, H.-K.; Ko, D.-H.; Yang, H.; Park, B. Additive-Free Hollow-Structured Co_3O_4 Nanoparticle Li-Ion Battery: The Origins of Irreversible Capacity Loss. *ACS Nano* **2014**, *8*, 6701−6712.
(28) Reddy, M. V.; Subba Rao, G. V.; Chowdari, B. V. R. Metal Oxides and Oxysalts as Anode Materials for Li Ion Batteries. *Chem. Rev.* **2013**, *113*, 5364−5457.
(29) Wang, Y.; Zhang, H. J.; Lu, L.; Stubbs, L. P.; Wong, C. C.; Lin, J. Designed Functional Systems from Peapod-Like Co@Carbon to Co_3O_4@Carbon Nanocomposites. *ACS Nano* **2010**, *4*, 4753−4761.
(30) Fu, L.; Chen, C.-C.; Maier, J. Interfacial Mass Storage in Nanocomposites. *Solid State Ionics* **2018**, *318*, 54−59.
(31) Sennu, P.; Aravindan, V.; Lee, Y.-S. High Energy Asymmetric Supercapacitor with 1D@2D Structured $NiCo_2O_4$@Co_3O_4 and Jackfruit Derived High Surface Area Porous Carbon. *J. Power Sources* **2016**, *306*, 248−257.
(32) Aravindan, V.; Lee, Y.-S.; Madhavi, S. Best Practices for Mitigating Irreversible Capacity Loss of Negative Electrodes in Li-Ion Batteries. *Adv. Energy Mater.* **2017**, *7*, 1602607.
(33) Zaghib, K.; Goodenough, J. B.; Mauger, A.; Julien, C. Unsupported Claims of Ultrafast Charging of $LiFePO_4$ Li-Ion Batteries. *J. Power Sources* **2009**, *194*, 1021−1023.
(34) Xu, Y.; Zhang, C.; Zhou, M.; Fu, Q.; Zhao, C.; Wu, M.; Lei, Y. Highly Nitrogen Doped Carbon Nanofibers with Superior Rate Capability and Cyclability for Potassium Ion Batteries. *Nat. Commun.* **2018**, *9*, 1720.
(35) Adekoya, D.; Li, M.; Hankel, M.; Lai, C.; Balogun, M.-S.; Tong, Y.; Zhang, S. Design of A 1D/2D C_3N_4/rGO Composite as an Anode Material for Stable and Effective Potassium Storage. *Energy Storage Mater.* **2020**, *25*, 495−501.
(36) Adekoya, D.; Gu, X.; Rudge, M.; Wen, W.; Lai, C.; Hankel, M.; Zhang, S. Carbon Nitride Nanofibres with Exceptional Lithium Storage Capacity: From Theoretical Prediction to Experimental Implementation. *Adv. Funct. Mater.* **2018**, *28*, 1803972.
(37) Dong, Y.; Xu, Y.; Li, W.; Fu, Q.; Wu, M.; Manske, E.; Kröger, J.; Lei, Y. Insights into the Crystallinity of Layer-Structured Transition Metal Dichalcogenides on Potassium Ion Battery Performance: A Case Study of Molybdenum Disulfide. *Small* **2019**, *15*, 1900497.
(38) Sennu, P.; Kim, H. S.; An, J. Y.; Aravindan, V.; Lee, Y. S. Synthesis of 2D/2D Structured Mesoporous Co_3O_4 Nanosheet/N-Doped Reduced Graphene Oxide Composites as a Highly Stable Negative Electrode for Lithium Battery Applications. *Chem. - Asian J.* **2015**, *10*, 1776−1783.

https://dx.doi.org/10.1021/acsnano.0c04950
ACS Nano 2020, 14, 10648−10654